Silicon (2023) 15:7797–7810
https://doi.org/10.1007/s12633-023-02620-2

RESEARCH

Sm^{3+}-Doped Alumino Borophospho-Silicate Glasses: An Examination of the Optical, Structural, and Gamma-ray Protective Features

M. N. Vishnu Narayanan Namboothiri[1] · K. A. Naseer[2] · K. Marimuthu[1] · Nouf Almousa[3] · M. I. Sayyed[4,5]

Received: 11 May 2023 / Accepted: 5 August 2023 / Published online: 14 August 2023

Abstract
A prime series of Sm^{3+}-doped alumino borophospho-silicate (xABPS) glasses were fabricated while varying the samarium ion concentration by employing the traditional melt-quenching method. XRD and FTIR characterizations were made for the structural investigation of the present glasses and the physical properties were calculated and reported. The high compactness and bonding nature of the xABPS glass system are explained through parameters such as boron–boron spacing, oxygen packing density, and the metallization criterion. The calculated mechanical properties illustrate the packing efficiency of the studied glasses. The absorption spectra exhibited several peaks in the UV–Vis-NIR region and following Tauc's plot method, the direct and indirect band gap for the glasses are determined and discussed. Various photon interaction parameters were calculated using the Phy-X program in a selected energy range. The obtained results of the studied glasses' mass attenuation coefficient (MAC), mean free path (MFP), and half-value layer (HVL) are compared with the reported data, whereby the increasing value of MAC, and the decreasing values of MFP and HVL confirm that the discussed glasses are suitable for radiation-shielding purposes.

Keywords Structural properties · Optical band gap · Optical basicity · Ionic character · Radiation shielding

1 Introduction

The elevated power diffusion depth and the enormous energy deposited on the target materials are the primary reasons of interest for scientists working with gamma rays [1]. The increasing electricity demand is resolved by the use of nuclear reactors, which extensively use the properties of gamma rays. The medical field, especially in cancer treatment, also exploits the properties of gamma rays. Furthermore, they have wide applicability in different areas such as the preservation of edible products, the analysis of elements, and agriculture, as well as space research [2–4]; however, these rays have harmful effects on living organisms. Over the past several decades, researchers have paid increasing attention to developing a promising material to address this problem. Materials that lower the energy of photons and their number are pertinent for shielding purposes. In the past, materials like concrete, alloys, and rocks [5, 6] were used for shielding purposes because of their ease of availability and for several more decades, the material employed for the prevention of radiation was lead. However, scientists were driven to seek a better material because of Pb's toxicity and lack of transparency [7]. In terms of applications for visible light and other related technologies, transparency became crucial, thus prompting scientists to concentrate on glass-based materials.

Scientists were persuaded to focus on glass materials for shielding applications due to their ease of manufacture and transparency. As glass has superior thermal and mechanical stability, it has been used as a prominent material to

✉ K. Marimuthu
mari_ram2000@yahoo.com

1 Department of Physics, The Gandhigram Rural Institute - Deemed University, Gandhigram 624302, India

2 Department of Physics, Farook College (Autonomous), Kozhikode 673632, India

3 Department of Physics, College of Science, Princess Nourah Bint Abdulrahman University, P.O. Box 84428, 11671 Riyadh, Saudi Arabia

4 Department of Physics, Faculty of Science, Isra University, Amman, Jordan

5 Department of Nuclear Medicine Research, Institute for Research and Medical Consultations, Imam Abdulrahman Bin Faisal University, P.O. Box 1982, 31441 Dammam, Saudi Arabia

safeguard humans from radiation [8]. Furthermore, studies have been carried out on glassy materials to enhance their shielding ability. There are several elements available on Earth with high glass-forming ability, such as SiO_2, B_2O_3, TeO_2, P_2O_5, and Sb_2O_3. Presently, borate is receiving much attention because of its special properties like the ease of manufacturing, high thermal stability, and cost-effectiveness. The strong bonding of boron with oxygen and the triangular and tetrahedral structure of BO_3 and BO_4 units have made B_2O_3 an excellent host for glass preparation [9]. Good stability, a better refractive index, and lower dispersion were realized when borate and silicate were added together. The multi-layer glass has more noteworthy properties than other glasses. A glass structure with comparatively high mechanical strength and high thermal stability is a necessity for radiation shielding, and a tri-former glass has much scope in the radiation-shielding field. The borosilicate glass structure seems to be unstable, probably because of the hygroscopic and sensitive nature of the borate toward the atmosphere. Alkali earth metals such as magnesium and calcium have been used as network modifiers, which in turn strengthen the glass structure by magnifying the mechanical properties. Moreover, magnesium possesses some interesting characteristics such as high thermal stability and high resistance to corrosive attack, which are more profitable for radiation dosimetry [10].

Aluminum oxide plays a key role in modifying the glass network and making the system more suitable for radiation protection. The formation of AlO_4 and AlO_6 units due to the incorporation of aluminum with borate will enhance the characteristics of the alumino–borate network. Moreover, Al_2O_3 improves the chemical resilience and metallic and optical properties of the shield [11]. Heavy metal oxides such as aluminum oxides help to form a more closely packed structure, which increases the density and refractive index of the glass.

The milestones in the investigations for proper shielding materials should be taken into account. A study on concrete technology in nuclear radiation shielding was started in 1989 by Kaplan. Then later, Makarious et al., Özen et al., and Sakr et al. [12–14] investigated heavyweight concrete and found more suitable properties for shielding. As the priorities changed to more focused applications, lead-based shielding materials became preferable. Furthermore, studies based on lead with polymers exhibit good results for shielding applications. The new era in radiation shielding started with the arrival of glass composites, and in 2005 Singh et al. suggested a better alternative for lead [15]. The Bi_2O_3 and BaO glasses can be used instead of PbO to avoid the harmful effect of lead on the environment [16]. Researchers working in the radiation-shielding field then sought more preferable materials with cost-effectiveness. Lakshminarayana et al. suggested borate composite glass with good thermal and structural properties [17], while Dong et al. proposed lithium zinc bismuth borate glass with the composition $50Bi_2O_3 + 15B_2O_3 + (35 - X)$ $ZnO + XLi_2O$ for radiation-shielding applications, with the latter's work showing higher shielding parameter values compared to ordinary hematite–serpentine and ilmenite–limonite concretes [18]. Later, the impact of rare earth (RE) on the glass matrix used for radiation shielding was considered. The investigations carried out by Wagh et al. revealed that lanthanides such as Sm^{3+}, Eu^{3+}, and Nd^{3+} have some impact on the nature of Pb fluoroborate glasses [19]. The dopant composition(s) increases the densities of the glasses. The half-value layer (HVL) and effective atomic number (Z_{eff}) indicate the enhanced shielding properties of the $PbF_2 - TeO_2 - B_2O_3 - RE_2O_3$ glass system. In 2020, Naseer et al. worked on the chemical composition $20TeO_2 + (50 - X)B_2O_3 + 29.5BaO + XBi_2O_3 + 0.5Er_2O_3$, whereby the ionic nature of the TBX glass and its lower two-photon absorption coefficient value predicted the possibility of using this glass for NLO applications, with these series of glasses also showing low mean free path (MFP) and HVL values, which confirmed their suitability for gamma attenuation [20]. From the general trend, it can be asserted that researchers will continue to explore new materials for radiation-shielding applications.

The present work investigated the change in structural and radiation-shielding properties of borophospho-silicate glass by varying the concentration of Sm^{3+} ions with Al_2O_3. The physical, structural, and photon interaction properties were calculated to discover a promising glass material for radiation shielding. Furthermore, the radiative parameters such as the linear attenuation coefficient (LAC) were calculated using the Phy-X software. Other parameters like the HVL and transmission factor (TF) were also determined to find the optimal glass for the prevention of radiation [21–24].

2 Experimental Method

2.1 Synthesis Process

High-purity analytical grade chemicals such as H_3BO_3, SiO_2, P_2O_5, CaO, MgO, NaF, ZnO, and Sm_2O_3 were used for the preparation of glass. All the chemicals utilized for the synthesis of alumino borophospho-silicate (xABPS) glasses were from Sigma Aldrich, which ensured their 99.99% purity. The designed composition was $37H_3BO_3 + 9SiO_2 + 10P_2O_5 + 15CaO + 7MgO + 10NaF + 7ZnO + (5 - x)$ $Al_2O_3 + xSm_2O_3$ and all the chemicals were taken in wt%. The concentration of Sm_2O_3 varied from 0.1 to 2 wt%. A batch of 15 gm was weighed and kept in an agate motor. The melting temperature was 1210 °C for 45 min. The molten flux was transferred to a preheated brass plate and placed

inside an annealing furnace at 400 °C. The present set of glasses belongs to the Boro-silicate host matrix, which has high phonon energy. So there is more possibility for breakage of the glasses. To increase the mechanical strength and thermal stability annealing has to be carried out for a long time. This annealing process strengthened the glass by enhancing its mechanical stability. After 8 h of annealing, the furnace was switched off and allowed to gradually reach room temperature. The prepared sets of glasses were removed and polished on both sides to obtain a uniform surface, and to avail optical quality.

2.2 Characterization

The densities of the well-polished aluminum borophosphosilicate glasses were determined using the Archimedes' principle. The immersion liquid used for this process was xylene. One of the requirements for the suspending liquid is to possess a relatively low surface tension, which typically excludes the use of water for accurate glass density determinations. Furthermore, water tends to hydrate the surface of the glass samples, which is also not convenient. Using Abbey refractometer instrumentation, the refractive index was estimated. The instrument details for the characterizations are detailed in [25–27].

3 Results and Outcome

3.1 Structural Analysis

To substantiate the amorphous nature of the fabricated xABPS glass system, the X-diffraction technique was utilized, with the XRD pattern of the xABPS glass shown in Fig. 1 as a representative case. The existence of wide scattering around the lower angles validates the non-crystalline nature of the prepared glass. The FTIR spectral analysis of the synthesized glasses was recorded and is shown in Fig. 2. Furthermore, the observations pertaining to the functional group analysis are presented in Table 1.

3.2 Physical Properties

The physical distinctiveness of the prepared aluminum borophospho-silicate glasses blended with Sm^{3+} ions is tabulated in Table 2. The replacement of aluminum with the Sm^{3+} RE ion, which has high molecular and atomic weight, might be a reason for the enhancement of density from 3.00 to 3.47 g/cm^3 in the xABPS glass system. The change in the B – O ratio due to the addition of RE ions causes an increase in BO_4 units and as a consequence, the compactness of the glass matrix increases [28]. As the density and molar volume shows contradictory trends, the V_M values decrease with

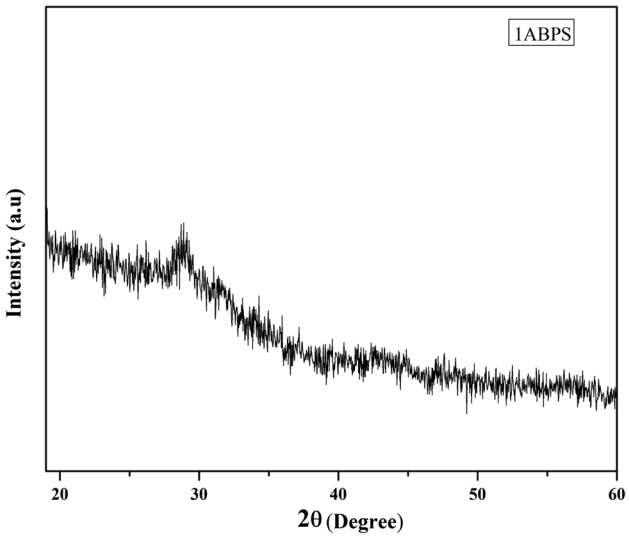

Fig. 1 XRD profile of the Sm^{3+} ion-doped xABPS glass

the increase in RE ions' concentration, thus, in turn, leading to a reduction in bond length and inter-ionic spacing. In comparison to other reported studies [29–31], the present work has similar or lower inter-ionic spacing, which indicates the higher rigidity of the prepared glasses. The appreciable de-escalation in the polaron radius and inter-ionic spacing reveals the compactness of the glass matrix. Reduction in inter ionic distance and polaron radius indicates the decreasing Sm–O distance, which accumulates a large number of Sm–O, thus compactness of the glass matrix increased. Moreover, due to the reduction in RE-oxygen separation, a considerable increase in the Sm – O bond strength will produce an intense field around the Sm^{3+} ions. These

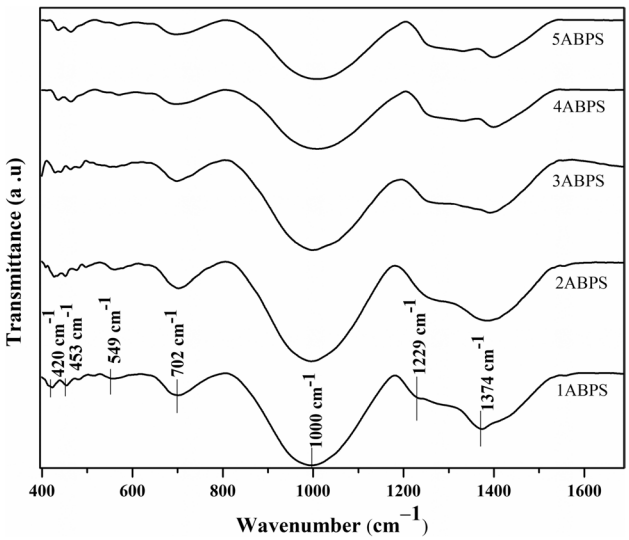

Fig. 2 FTIR spectra of the Sm^{3+} ion-doped xABPS glasses

Table 1 Band positions (cm^{-1}) and the corresponding peak assignments of the FTIR spectra of the Sm^{3+} ion-doped xABPS glasses

Sl. No	1ABPS	2ABPS	3ABPS	4ABPS	5ABPS	Band assignment
1	1374	1384	1392	1396	1398	B-O stretching vibrations of trigonal $[BO_3]^{3-}$ units
2	1229	1251	1257	1259	1263	Anti-symmetric Si–O stretching vibrations
3	1000	997	999	1001	1003	Stretching modes of B–O bond which could form tri-, tetra-, penta-borate groups
4	702	696	698	694	692	Al-O stretching vibrations of AlO_5 groups
5	549	557	562	565	569	Bending modes of $[PO_4]^{3-}$ units
6	453	453	465	463	467	Si–O-Si bending vibrations

intense field strengths were computed using the expression $F = Z/r_p^2$ (Z-atomic number of Sm^{3+}, r_p-polaron radius) [32]. Another fundamental parameter of interest for glass is the refractive index (n_d), which is experimental and estimated using the Abbe refractometer instrumentation technique, whereby among the prepared glasses the ABPS2Sm glass shows a higher value. The Sm^{3+} ions' concentration in the prepared set of glasses was estimated from the Bond density (n_b) values. Furthermore, the deduction of non-bridging oxygens in the glass matrix could easily be understood by the lessening electronic polarizability values. The greater the bonding oxygen, the less the polarizability; this reveals the high compactness of the glass [33]. The molar refractivity values were calculated from the n_b values, and appeared to be lowering with the increase in RE ions' concentration. The amount of incident radiation that gets reflected at the surface of the glass is termed reflection loss. Glasses with less compactness allow the radiation to transmit more radiation through it so that the reflection loss value decreases. Hence the increasing value of reflection loss in the present work indicates the increasing compactness of the glasses. The steady rise in reflection loss values (R,%) validates the compactness of the xABPS glass system.

3.3 Structural Properties

Apart from the FTIR analysis, a comprehensive investigation of the structural features of the prepared xABPS glass system was necessary. A theory put forward by Dimitrov et al. [34] explains the metallization criteria of metals and insulators. The value of M implicates the nature of the material, whereby a positive and lower magnitude of M suggests the non-metallic character of the glass. The value of the metallization constant relies on the parameters of density and molar refractivity. The present set of glasses contains multiple former oxides such as boron, phosphate, and silicate. Since the domination of boron (in wt%) in the host network is higher, the separation of boron ions itself will expose the compactness of the glass matrix. The consistent decrement in the boron–boron separation values with the increase of Sm^{3+} ions' concentration confirms the higher compactness of the glass system. In addition, the parameters like oxygen molar volume (V_o) and oxygen packing density (OPD) were estimated and tabulated using the expressions reported in the literature [35–37]. Figure 3 depicts the correlation of d_{B-B}, V_o, and OPD with the increment in the RE ions' concentration. The V_o values manifest a reverse trend, in comparison

Table 2 Physical properties of the Sm^{3+} ion-doped xABPS glasses

Sl. No	Physical properties	1ABPS	2ABPS	3ABPS	4ABPS	5ABPS
1	Density, ρ (g/cm^3)	3.009	3.103	3.220	3.301	3.477
2	Refractive index, n_d	1.661	1.665	1.669	1.672	1.678
3	Average molecular weight, M_T (g)	75.944	76.314	76.932	78.165	80.633
4	Molar volume, V_M (cm^3)	25.239	24.588	23.886	23.674	23.183
5	RE ion concentration, N (10^{20} ions/cm^3)	0.504	1.283	2.642	5.327	10.865
6	Polaron radius, r_p (Å)	10.93	7.98	6.28	4.97	3.91
7	Inter ionic distance, r_i (Å)	27.14	19.82	15.58	12.34	9.72
8	Field strength, F (10^{16} cm^{-2})	0.73	1.39	2.26	3.65	5.83
9	Electronic polarizability, α_e (10^{-24} cm^3 /mol)	3.416	3.344	3.264	3.246	3.201
10	Molar refractivity, R_m (cm^{-3})	9.328	9.131	8.912	8.864	8.741
11	Dielectric constant, (ε)	2.758	2.772	2.785	2.795	2.815
12	Reflection losses, R (%)	6.170	6.226	6.283	6.325	6.409
13	Optical dielectric constant, χ_{opt}	1.865	1.854	1.846	1.841	1.830

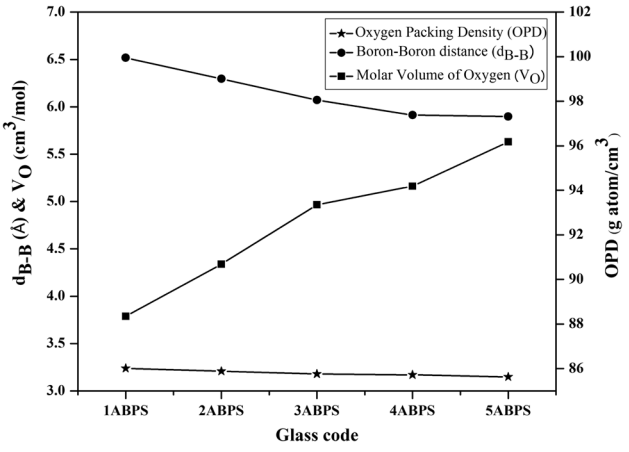

Fig. 3 The variation of boron–boron separation (d_{B-B}), molar volume of oxygen (V_o), and OPD of the Sm^{3+} ion-doped xABPS glasses

with the other two. This also points to the compactness of the glass structure, with the confirmation of reducing the amount of non-bridging oxygen and the augmentation of bridging oxygen [38, 39]. The average coordination number and bond density were calculated from the following equations:

$$n_{av} = \sum_i (xn_c)_i$$

$$n_b = \frac{N_A}{V_m} \sum_i (xn_c)_i = \frac{N_A}{V_m} n_{av}$$

where NC is the coordination number of the cation, V_m molar volume, and N_A Avogadro number [40]. The slight variation in the average coordination number n_{av} ranges from 4.303 to 4.341; the bond density n_b values found had increasing ranges from 1.027 to 1.127×10^{24} m^{-2}, and the fall in the average single bond strength B_{M-O} values thus confirms that the structural modification takes place in the chosen configuration of the glass. The structural properties of the Sm^{3+} ion-doped glasses were calculated and are presented in Table 3.

3.4 Optical Electronegativity (χ_{opt}), Covalency, and Iconicity

The idea of the chemical bonding of the compounds can be correlated with the optical electronegativity (ΔX), where its magnitude ascribes the iconic and covalent nature of the chemical bond [41], and the mechanism for calculating the ΔX was deducted from the literature [42]. A noticeable result observed in the table is that the higher value of electronegativity illustrates the increase in the iconicity of the glasses. The iconicity (I_c) and the covalency (C_c) values were estimated using the following equations:

$$C_{ionic}(I_c, \%) = \left[1 - exp\left\{-0.25\left(\Delta\chi^2\right)\right\}\right] \times 100$$

$$C_{covalent}(C_c, \%) = exp\left\{-0.25\left(\Delta\chi^2\right)\right\} \times 100$$

The value of I_c greater than 90% validates the ionic character of the glass. Another criterion regarding the nature of the glass is optical basicity (Λ_{th}), which elucidates the ability of an oxygen atom to donate an electron in the oxides of the glass. The equation used for the theoretical calculation of basicity is taken from the literature [43]. There is a slight increment in Λ_{th} values for the present set of glasses. Eventually, the parameters like the optical basicity, electronegativity, and iconicity values of the studied glasses point toward an iconic nature other than a covalent one. The electronegativity (ΔX), ionic character factor (I_c,%), and covalent character factor (C_c,%) of the Sm^{3+} ion-doped studied glasses were calculated and are presented in Table 4.

3.5 Elastic Properties

The mechanical properties of amorphous materials receive more attention due to their technological applications. Elastic moduli such as the Young's modulus, shear modulus, bulk

Table 3 Structural properties of the Sm^{3+} ion-doped xABPS glasses

Sl. No	Structural properties	1ABPS	2ABPS	3ABPS	4ABPS	5ABPS
1	Metallization criterion, M	0.630	0.628	0.626	0.625	0.622
2	Boron–boron distance, d_{B-B} (Å)	3.24	3.21	3.18	3.17	3.15
3	Distribution density of boron, D_B	1.28	1.30	1.33	1.34	1.36
4	Oxygen packing density, OPD (g atom/cm^3)	88.35	90.69	93.35	94.19	96.18
5	Molar volume of oxygen, V_o (cm^3/mol)	6.518	6.295	6.071	5.913	5.856
6	Average coordination number, n_{av}	4.303	4.304	4.310	4.321	4.341
7	Bond density, n_b ($\times 10^{27}$ m^{-3})	1.027	1.027	1.086	1.099	1.127
8	Average single bond strength, B_{M-O} (KJ/mol)	233.03	232.73	232.45	231.85	230.73

Table 4 Electronegativity (ΔX), ionic character factor (I_c,%), and covalent character factor (C_c,%) of the Sm^{3+} ion-doped xABPS glasses

Glass chemical	ΔX	I_c %	C_c %
B_2O_3	6.24	99.994	0.005
SiO_2	4.98	99.797	0.202
P_2O_5	12.82	100	1.4E − 16
CaO	2.44	77.426	22.573
MgO	2.13	67.832	32.167
NaF	3.05	90.227	9.772
ZnO	1.79	55.113	44.886
Al_2O_3	7.1	99.997	0.003
Sm_2O_3	7.98	100	1.2E − 05
$37B_2O_3 + 9SiO_2 + 10P_2O_5 + 15CaO + 7MgO + 10NaF + 7ZnO + 4.9Al_2O_3 + 0.1Sm_2O_3$		90.22	9.77
$37B_2O_3 + 9SiO_2 + 10P_2O_5 + 15CaO + 7MgO + 10NaF + 7ZnO + 4.75Al_2O_3 + 0.25Sm_2O_3$		90.28	9.73
$37B_2O_3 + 9SiO_2 + 10P_2O_5 + 15CaO + 7MgO + 10NaF + 7ZnO + 4.5Al_2O_3 + 0.5Sm_2O_3$		90.36	9.61
$37B_2O_3 + 9SiO_2 + 10P_2O_5 + 15CaO + 7MgO + 10NaF + 7ZnO + 4Al_2O_3 + 1Sm_2O_3$		90.43	9.52
$37B_2O_3 + 9SiO_2 + 10P_2O_5 + 15CaO + 7MgO + 10NaF + 7ZnO + 3Al_2O_3 + 2Sm_2O_3$		90.47	9.36

modulus, and longitudinal modulus of the xABPS glasses were determined using formulas reported in the literature [44, 45]. All the calculated parameters are presented in Table 5. The Ym, Bm, Sm, and Lm modulus values show an increasing trend, and the 5ABPS glass exhibits a higher value. The increasing magnitude of the elastic moduli has a direct connection with the increase in the number of bridging oxygens, which in turn makes the glass more rigid [46]. Moreover, the packing efficiency of the studied glasses is explained through the atomic packing factor (APF) parameter values, while the higher and increasing trend suggests the compactness of the glass. The Poisson's ratio (μ_{cal}) values explain the deformation of the glass matrix, and follows the trend 5ABPS > 4ABPS > 3ABPS > 2ABPS > 1ABPS in the present set of glasses. The μ_{cal} values are one of the significant parameters that correspond to the compactness of the glass matrix in respect to the cross-linkage density. The calculated μ_{cal} values of the present glasses (0.354–0.367) suggest the moderate cross-linkage of the chosen glass configuration. Fractal bond connectivity defines the dimensionality changes in the glass configuration and the values range from 1.371 to 1.239, illustrating the two-dimensional layer structure. All the present glasses possess nearly the same hardness and the variation of H_m, f_D, and μ_{cal} with RE ions' concentration is exhibited in Fig. 4.

3.6 Optical Properties

Broad optical investigations of the prepared Sm^{3+}-doped glasses titled xABPS were carried out. The absorption spectra of the samarium oxide-incorporated glasses were recorded at ambient temperature in the 400 – 2000 nm wavelength range and are presented in Fig. 5. It is observed from the absorption spectrum that twelve major transition peaks each originate from the $^6H_{5/2}$ ground state to different excited states, illustrating the f – f transitions. The bands $^6P_{3/2}$, $^4G_{9/2}$, $^4M_{5/2}$, $^4F_{3/2}$, and $^4G_{5/2}$ are observed around 401, 436, 474, 527, and 562 nm, respectively, in the visible region. Whereas in the NIR region, the seven well-defined bands $^6F_{11/2}$, $^6F_{9/2}$, $^6F_{7/2}$, $^6F_{5/2}$, $^6F_{3/2}$, $^6H_{15/2}$, and $^6F_{1/2}$ are observed around 942, 1075, 1230, 1371, 1474, 1525, and 1581 nm, respectively. The spectral profile in the present work exhibits a similar trend on par with the reported literature [47]. In the present investigation, it is observed that the transitions $^6P_{3/2}$ and $^6F_{7/2}$

Table 5 Elastic properties of the Sm^{3+} ion-doped xABPS glasses

Sl. No	Elastic properties	1ABPS	2ABPS	3ABPS	4ABPS	5ABPS
1	Poisson's ratio, μ_{cal}	0.354	0.358	0.362	0.364	0.367
2	Atomic packing fraction, APF	0.966	0.989	1.021	1.023	1.056
3	Young's modulus, E_t (GPa)	50.01	51.13	52.94	53.56	55.00
4	Bulk modulus, K_t (GPa)	57.14	59.84	63.98	65.45	68.9
5	Shear modulus, S_t (GPa)	19.6	19.92	20.62	20.84	21.35
6	Longitudinal modulus, L_t (GPa)	83.27	86.4	91.47	93.23	97.36
7	Microhardness, H_m (GPa)	1.789	1.781	1.780	1.779	1.778
8	Fractal bond connectivity (f_D)	1.371	1.331	1.289	1.273	1.239

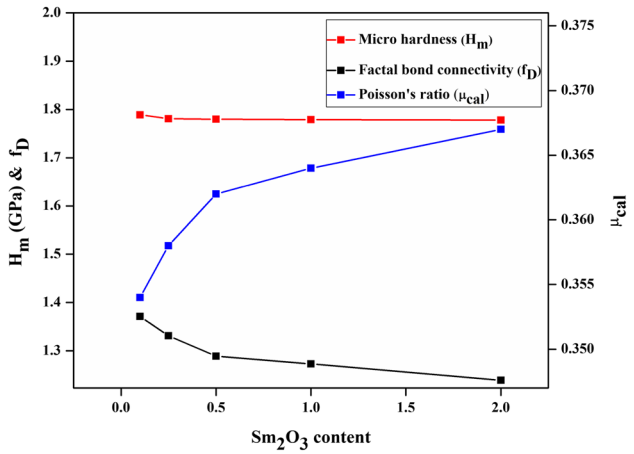

Fig. 4 The variation of Poisson's ratio (μ_{cal}), micro hardness (H_m), and fractal bond connectivity (f_D) of the Sm^{3+} ion-doped xABPS glasses as a function of an increasing order of Sm^{3+} ions' concentration

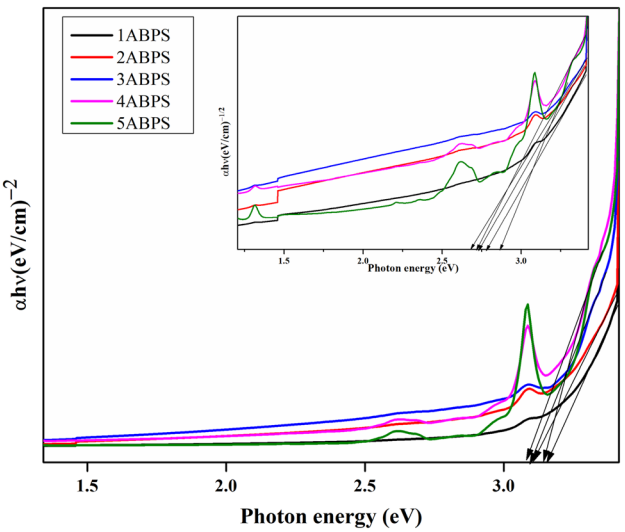

Fig. 6 Tauc's plot for the direct allowed transition in the Sm^{3+} ion-doped xABPS glasses (Inset shows the Tauc's plot for the indirect allowed transition)

are much more intense compared to the other bands, and are designated as hypersensitive transitions that follow the selection rule $|\Delta J| \leq 6$ and $|\Delta J| = 0, \pm 1$ [48].

Optical absorption studies have conspicuous advantages in terms of perceiving the glassy materials' richness in various applications. The electronic band structure of the amorphous materials can be determined through a keen examination of the optical band gap. The band gap values for the direct and indirect allowed transitions were estimated following the Mott and Davis theory, as elucidated in the literature [49]. Tauc's plot of the present set of glasses for the direct and indirect band gap estimation is portrayed in Fig. 6. The optical energy gap for each of the glasses in the xABPS set is tabulated in Table 6. There is a noticeable de-escalation in the direct and indirect values, and the 3ABPS glass shows less band gap value among the prepared glasses. The coagulation of electrons at the conduction band is referred to as Urbach's energy (ΔE). The degree of disorderliness of the amorphous materials was assessed through the ΔE values, as the localized density states in glassy materials are correlated to their long-range order. The tail width of the localized states gives the ΔE. The Urbach's energy was found to be lower in the glass with 0.5% Sm_2O_3 concentration and higher in the glass with 1% Sm_2O_3 concentration.

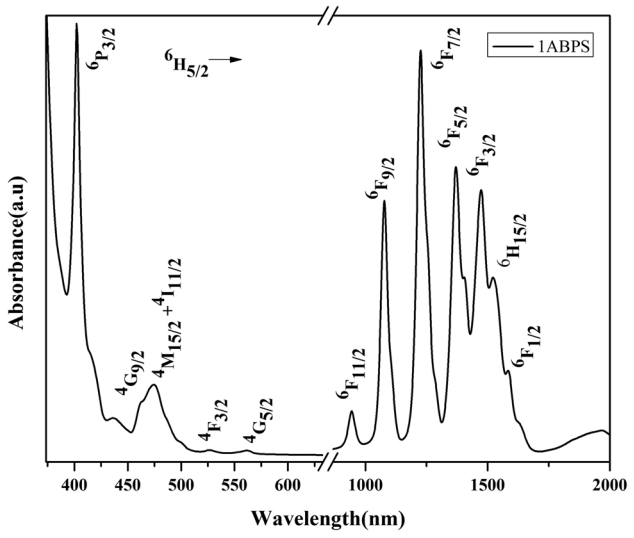

Fig. 5 Absorption spectrum of the Sm^{3+} ion-doped xABPS glass

3.7 Radiation Attenuation Exceptionality

The theoretical values of mass attenuation coefficient (MAC) for the chosen 1ABPS, 2ABPS, 3ABPS, 4ABPS, and 5ABPS glasses are provided in Fig. 7. These values were calculated using the Phy-X program [50] between 0.015 and 15 MeV. The variation in the MAC with the energy for the aforementioned glasses was found to be identical. Except for 0.05 MeV, the 1ABPS, 2ABPS, 3ABPS, 4ABPS, and 1ABPS samples display a declining trend in the MAC. Three key principles explaining how photons interact with the glass are strongly connected to the current behavior of the MAC with energy [24]. The maximum MAC was found at 0.015 MeV (ranging from 11.53 to 17.38 cm^2/g), and after that, the MAC significantly decreases up to 0.05 MeV. When the energy goes from 0.015 to 0.05 MeV, the MAC drops from 11.52 to 0.582 cm^2/g for 1ABPS and from 17.38 to 1.92 cm^2/g for 5ABPS. With the help of the photoelectric absorption

Table 6 Bandgap and Urbach energy values of the Sm^{3+} ion-doped xABPS glasses

Glass code	Transition from $^6H_{15/2} \rightarrow$			
	Absorption edge λ_{edge} (nm)	Direct bandgap E_1 (eV)	Indirect bandgap E_2 (eV)	Urbach energy ΔE (eV)
1ABPS	418	3.15	2.78	1.16
2ABPS	413	3.20	2.74	1.36
3ABPS	412	3.07	2.67	0.35
4ABPS	410	3.15	2.72	1.77
5ABPS	407	3.13	2.86	0.81

(PEA) mechanism, such a pattern in the MAC may be seen. It is important to note that the following is how this phenomenon's chance might be expressed:

$$\tau\alpha\frac{Z^{4-5}}{E^3} \tag{1}$$

According to this relationship, when low-energy photons are taken into account, the likelihood of PEA occurring is high. Additionally, the high atomic number of Sm present in these glasses greatly increases the likelihood of PEA occurring. Additionally, all of the chosen glasses have approximately the same MAC of between 0.3 and 3 MeV, indicating that the composition of the samples has little effect on the attenuation trend between these energies. Compton scattering (CS), which is crucial for these energies, is mostly responsible for this pattern in the MAC. As is well known, the likelihood of CS is almost independent of the shielding materials' atomic number (Z). The 1ABPS–5ABPS glasses, for instance, have MAC values of around 0.045 cm^2/g at 2 MeV. Additionally, a very slight decrease in the MAC is seen for E greater than 4 MeV, which is due to the pairing creation (PP). As the amount of Sm_2O_3 grows, it can be seen from Fig. 7 that the MAC increases. The highest MAC values are seen in 5ABPS, which contains 2 mol% Sm_2O_3. This can be explained by the fact that Sm has a greater atomic number than Al. 5ABPS demonstrates greater radiation absorption performance than the 1ABPS–4ABPS samples.

Moreover, in Fig. 8 we show the LAC to study the energy and density dependency on the photon attenuation capabilities for the evaluated 1ABPS–5ABPS samples with various amounts of Sm_2O_3. It is shown that the energy and ratios of Sm_2O_3 have a significant impact on the LAC for the 1ABPS–5ABPS samples. The glass with high LAC can absorb more photons than the glass with low LAC, which is a significant consideration. As a result, a high amount of photons can pass through glass having low LAC. This information will enable us to determine the most effective gamma photon shield. When the amount of S_2O_3 is increased from 0.1 to 2 mol%, the density shifts from 3.009 to 3.477 g/cm^3. According to Fig. 8, increasing the concentration of Sm_2O_3 from 0.1 mol% (1ABPS) to 2 mol% (5ABPS) causes the

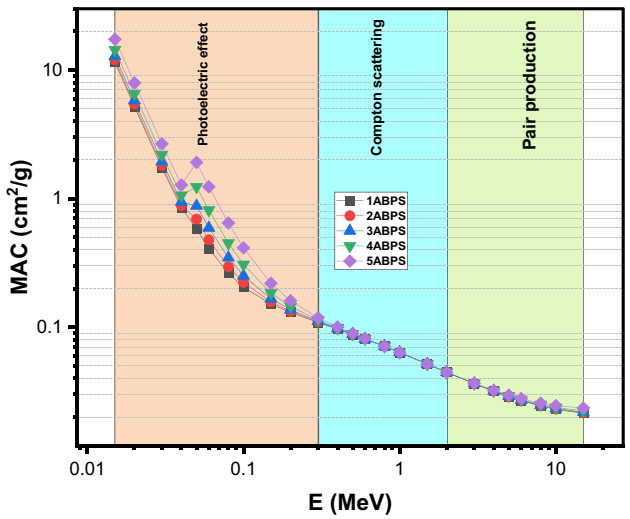

Fig. 7 Theoretical MAC values for the chosen 1ABPS, 2ABPS, 3ABPS, 4ABPS, and 5ABPS glasses

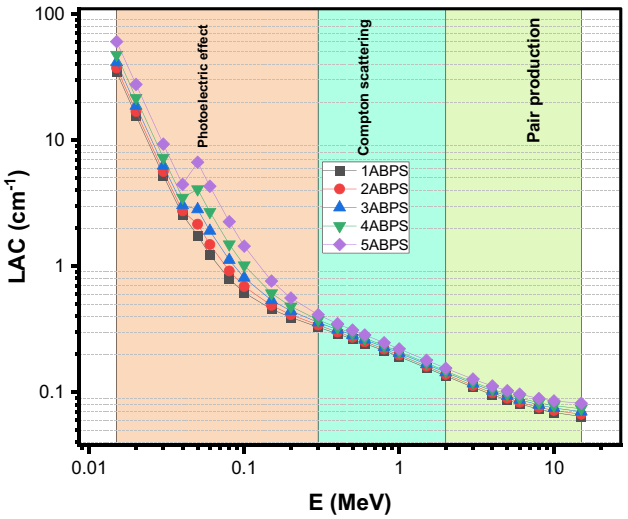

Fig. 8 Theoretical LAC values for the chosen 1ABPS, 2ABPS, 3ABPS, 4ABPS, and 5ABPS glasses

LAC to increase, which enhances the shielding efficiency for the studied samples. The 1ABPS–5ABPS glass systems' photon attenuation properties were significantly impacted by the density. Since the atoms in the high-density samples are relatively close together, photons interact with them and lose some of their energy as a result. This illustrates the rationale for the 5ABPS glass's maximum photon attenuation characteristics. As a result, the LAC values and hence the shielding performance are greatly influenced by the sample density. Furthermore, based on Fig. 8, we can conclude that the shielding potentiality tends to decline from 0.015 to 15 MeV. This is due to the LAC's very high initial values (34.68, 37.29, 41.29, 47.51, and 60.42 cm^{-1} at 0.015 MeV), which are subsequently followed by a gradual reduction up to 0.1 MeV and then a slight decrease up to 15 MeV. Additionally, a peak is observed around 0.05 MeV close to the K edge of Sm.

Additionally, by applying the concept of the Z_{eff}, it is conceivable to predict how well the tested 1ABPS–5ABPS glasses with varied concentrations of Sm_2O_3 will function as a shielding material. In Fig. 9, the predicted Z_{eff} values for the glasses under test are displayed between 0.015 and 15 MeV. The Z_{eff} figure for the investigated glasses can be separated into three groups. First, E < 0.1 MeV, whereby in this range, the Z_{eff} values have the largest value and range between 19.03–10.34, 19.67–11.43, 20.71–13.16, 22.65–16.29, and 26.07–21.51 for the 1ABPS–5ABPS glasses, respectively. The PEA is strongly reliant on the atomic number, and the presence of S_{min} in the specimens increases the likelihood that PEA will occur. As a result, the dominance of PEA in this area is linked to the trend in Z_{eff} in this region. We noticed the high value of Z_{eff}, particularly at 0.015 MeV, and for the sample with 2 mol% of Sm_2O_3 (i.e. 5ABPS). It is obvious that the Z_{eff} rapidly decreases between 0.01 and 1.5 MeV, which represents the second region, where Z_{eff} reaches minimal values at 1.5 MeV (equal to 7.51, 7.55, 7.61, 7.73, and 7.97 for 1ABPS–5ABPS, respectively). The third region is E > 1.5 MeV, where the Z_{eff} grows once more up to 15 MeV. The 5ABPS sample, on the other hand, exhibits maximum Z_{eff} values due to its composition of 37H_3BO_3-9SiO_2-10P_2O_5-15CaO-7MgO-10NaF-7ZnO-3Al_2O_3-2Sm_2O_3. This glass has 2 mol% Sm_2O_3, whereas the other glasses have less Sm_2O_3.

Using the HVL, the gamma-ray penetration strength through the chosen 1ABPS–5ABPS glasses may be taken into consideration. This factor typically denotes the thickness of the medium (in this case, the H_3BO_3-SiO_2-P_2O_5-CaO-MgO-NaF-ZnO-Al_2O_3-Sm_2O_3 glasses) that is penetrated by half of the photons and is quantified in units of thickness (mm or cm). As is well known, the potential for attenuation is significant for high-density samples, and as a result, the HVL is minimal. In practical applications, it is preferable to use glass with a low HVL, which can be accomplished by utilizing heavy metal oxides. Figure 10 displays the HVL findings for the chosen samples as determined by the Phy-X software. This figure clarifies that the HVL decreases as the Sm_2O_3 level is changed from 0.1 to 2 mol%, thus signifying that the examined glasses have varying shielding efficiencies, with the 5ABPS glass having the best shielding efficiency (corresponding to 2 mol% of Sm_2O_3 and the highest density), while the 1ABPS glass has the worst. With respect to 0.015, 0.04, 0.15, 0.8, 2, 4,

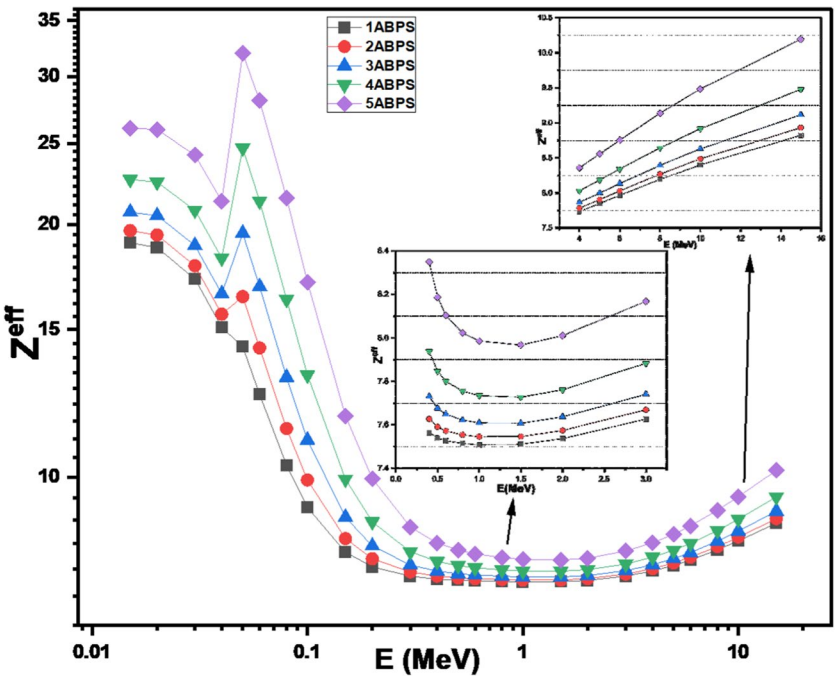

Fig. 9 The Z_{eff} for the chosen 1ABPS, 2ABPS, 3ABPS, 4ABPS, and 5ABPS glasses

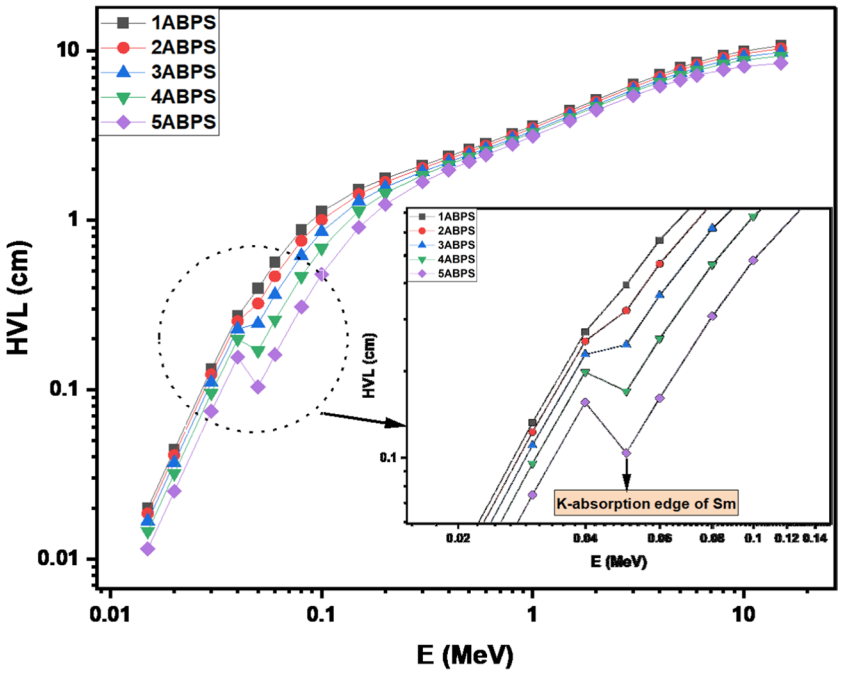

Fig. 10 The HVL for the chosen 1ABPS, 2ABPS, 3ABPS, 4ABPS, and 5ABPS glasses

and 8 MeV, the 1ABPS's HVL is 0.020, 0.272, 1.521, 3.247, 5.151, 7.244, and 9.448 cm, respectively. The HVL values for the 5ABPS glass are 0.011, 0.156, 0.908, 2.806, 4.474, 6.174, and 7.760 cm for the abovementioned energies. This means that for the denser material, a thin sample can be employed to shield the radiation, whereas for the low-density specimen, a thick specimen is required to block the incoming radiation. Additionally, it is clear from Fig. 10 that the HVL considerably alters as the photon energy changes. The sample's thickness becomes increasingly important as the photons' energy rises to reduce their intensity. In particular, the HVL for 2ABPS is 0.019 and 9.121 cm at 0.015 and 8 MeV, respectively, while the 4ABPS's HVL values are 0.015 and 8.391 cm at these energies.

The MFP data were used to estimate the effect of Sm_2O_3 on the radiation-protection capabilities of the investigated glasses. Mean free path (MFP) is the average distance traveled by an incident particle (photon) before each successive

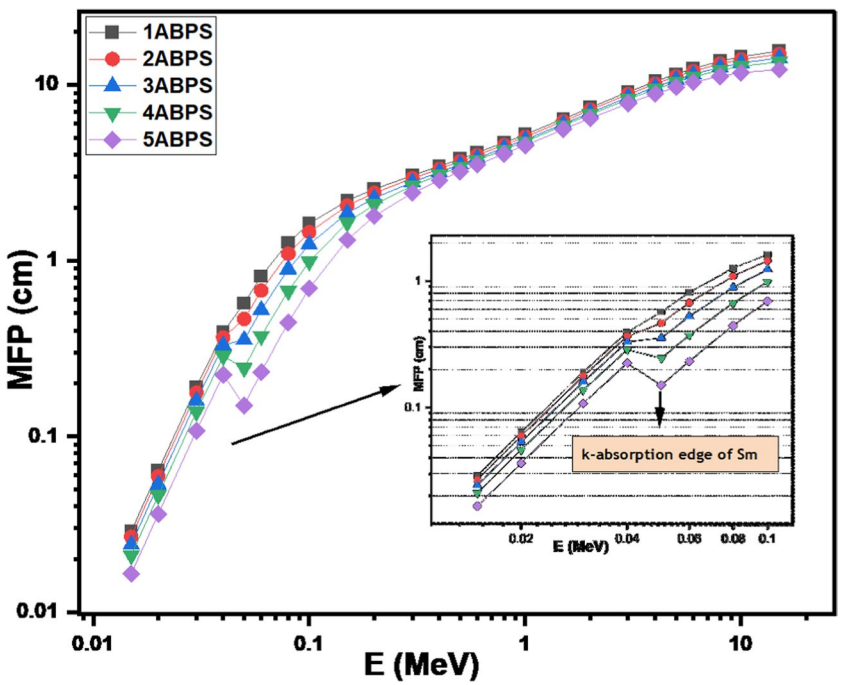

Fig. 11 The MFP for the chosen 1ABPS, 2ABPS, 3ABPS, 4ABPS, and 5ABPS glasses

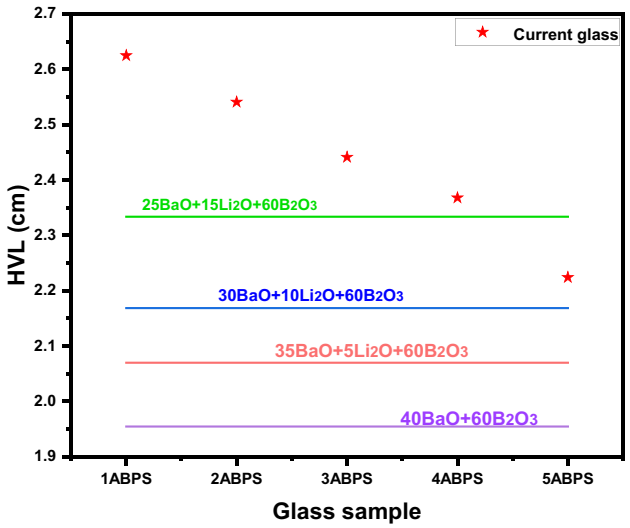

Fig. 12 The HVL for the chosen glasses in comparison with the BaO-Li_2O-B_2O_3 glasses

collision with particle present in the glasses. Lower MFP indicates more frequent collisions and so more often the incident radiation losses its energy and gets attenuated. To create materials with adequate protection, the designers of shielding materials and glasses typically utilize some HMO to reduce the MFP as much as possible. In Fig. 11, the MFP findings for the 1ABPS–5ABPS samples assessed by Phy-X are plotted. The results for the MFP are comparable to those for the HVL, apart from a change in magnitude. High-energy photons may easily pass through the 1ABPS–5ABPS samples, as shown by the MFP curves, since the MFP rises as the photon energy increases. The smallest MFP, ranging from 0.029 cm (1ABPS) to 0.017 cm (5ABPS) is seen at 0.015 MeV. For the 1ABPS–5ABPS samples, the MFP was determined to be 1.265, 1.093, 0.893, 0.671, and 0.444 cm, respectively, at 0.08 MeV. According to Fig. 11, the MFP drops as Sm_2O_3 is added, and 5ABPS has the lowest MFP while 1ABPS has the highest. For the 1ABPS and 5ABPS samples, we compared the effect of Sm_2O_3 on the MFP at various energy levels, including 0.015, 0.06, 0.5, 3, and 8 MeV. We found that the MFP for 1ABPS is higher than that of 5ABPS by 1.74-, 3.49-, 1.18-, 1.16-, and 1.21-fold, which means that when the amount of Sm_2O_3 rises from 0.1 to 2 mol%.

We show the HVL for the 1ABPS–5ABPS samples in Fig. 12, together with BaO-Li_2O-B_2O_3 glasses for the sake of comparison [51]. The HVL of the 5ABPS glass, according to these findings, is less than that of the 25BaO-16Li_2O-60B_2O_3 sample, although the HVL of the 4ABPS sample is relatively near to that of 25BaO-16Li_2O-60B_2O_3. The 1ABPS–3ABPS glasses have higher MFP than all the BaO-Li_2O-B_2O_3 glasses. In Fig. 13**,** we compare the HVL for the 1ABPS–5ABPS samples with CaF_2-BaO-P_2O_5 glasses [52]. According to the results, 5ABPS possesses almost the same HVL as 8CaF_2-42BaO-50P_2O_5, while the other glasses in this work have higher HVL than all the CaF_2-BaO-P_2O_5 glasses. In Fig. 14**,** we compare the HVL for the chosen glasses in comparison with the B_2O_3-V_2O_5-BaF_2-Na_2O glasses [53]. The 3ABPS sample has an HVL close to 59B_2O_3-1V_2O_5-20BaF_2-20Na_2O, while 4ABPS has an almost comparable HVL with 58B_2O_3-2V_2O_5-20BaF_2-20Na_2O, and 5ABPS has a lower HVL than all the B_2O_3-V_2O_5-BaF_2-Na_2O glasses.

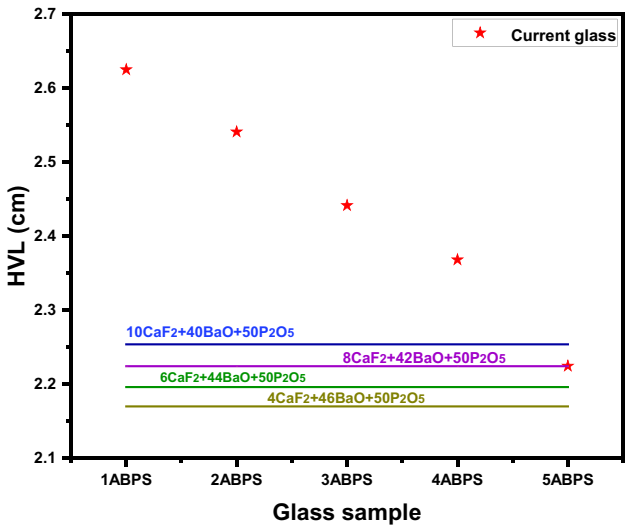

Fig. 13 The HVL for the chosen glasses in comparison with the CaF_2-BaO-P_2O_5 glasses

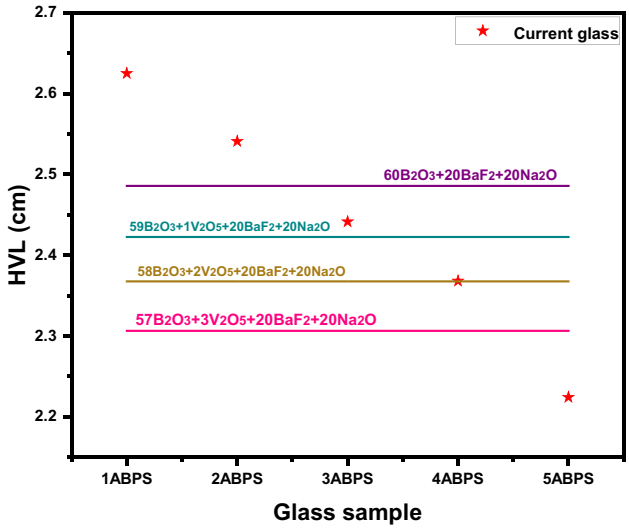

Fig. 14 The HVL for the chosen glasses in comparison with the B_2O_3-V_2O_5-BaF_2-Na_2O glasses

4 Conclusion

The physical, structural, mechanical, and radiation-shielding features of the present Sm^{3+}-doped glasses were reported and discussed. The confirmation of amorphous and the presence of various functional units in the studied glasses was recognized by XRD and FTIR characterizations, respectively. The noticeable decrement in the polaron radius and inter-ionic spacing with an increment in density showed the rigidity of the glass. Structural investigations illustrated the formation of bridging oxygen and the compactness of the glass network. The lowering value of the metallization criterion indicated the non-metallic characteristic, and the iconic nature of the prepared glass was demonstrated by the electronegativity and iconicity parameters. The mechanical properties such as the elastic moduli, APF, and Poisson's ratio provided clarity regarding the packing efficiency of the xABPS glasses. Various photon interaction parameters were calculated using the Phy-X program between 0.015 and 15 MeV. The 5ABPS sample demonstrated greater radiation absorption performance than the 1ABPS–4ABPS samples. The energy and ratios of Sm_2O_3 had a significant impact on the LAC for the 1ABPS–5ABPS samples. Moreover, the present glasses showed superior performance than the reported glass composition when the HVL and MFP were compared. From the detailed investigation of the physical, structural, mechanical, and radiation-shielding properties of the present set of glasses, the 5ABPS sample among the studied xABPS glasses was found to be a prominent material for radiation-shielding purposes.

Acknowledgements The authors express their gratitude to Princess Nourah bint Abdulrahman University Researchers Supporting Project number (PNURSP2023R111), Princess Nourah bint Abdulrahman University, Riyadh, Saudi Arabia.

Author Contributions All authors contributed to the study conception and design. Material preparation is done by Mr. M.N. Vishnu Narayanan Namboothiri, and data collection and analysis were performed by Mr. M.N. Vishnu Narayanan Namboothiri, Dr. K.A. Naseer and Dr. M.I. Sayyed. The first draft of the manuscript was written by Mr. M.N. Vishnu Narayanan Namboothiri, Dr. M.I. Sayyed and Dr. K.A. Naseer. The review and editing is done by Dr. K. Marimuthu and Dr. Nouf Almousa. The supervision is done by Dr. K. Marimuthu. All authors commented on previous versions of the manuscript. All authors read and approved the final manuscript.

Data Availability The datasets generated during and/or analysed during the current study are available from the corresponding author on reasonable request.

Declarations

Ethics Approval Authors declare under their ethical and legal responsibility that the submitted paper is original and is not being submitted for the peer review process in any other journal. This article does not contain any studies with human participants or animals performed by any of the authors.

Consent to Participate Informed consent was obtained from all individual participants included in the study.

Consent for Publication All authors read and approved the final manuscript for the publication.

Competing Interests The authors declare no competing interests.

References

1. Singh GP, Singh J, Kaur P et al (2020) Analysis of enhancement in gamma ray shielding proficiency by adding WO_3 in Al_2O_3-PbO-B_2O_3 glasses using Phy-X/PSD. J Mater Res Technol 9:14425–14442. https://doi.org/10.1016/j.jmrt.2020.10.020
2. Mohsin MH, Qureshi K, Ashfaq T (2019) Safety assessment of MSR concept using INPRO methodology. Prog Nucl Energy 117:103099. https://doi.org/10.1016/j.pnucene.2019.103099
3. Khandaker MU, Bradley DA, Osman H et al (2022) The significance of nuclear data in the production of radionuclides for theranostic/therapeutic applications. Radiat Phys Chem 200:110342. https://doi.org/10.1016/j.radphyschem.2022.110342
4. Yasmin S, Khandaker MU, Bradley DA et al (2022) The efficacy of various thicknesses of float glasses for protection of gamma-radiation. Radiat Phys Chem 199:110301. https://doi.org/10.1016/j.radphyschem.2022.110301
5. Libeesh NK, Naseer KA, Mahmoud KA et al (2022) Applicability of the multispectral remote sensing on determining the natural rock complexes distribution and their evaluability on the radiation protection applications. Radiat Phys Chem 193:110004. https://doi.org/10.1016/j.radphyschem.2022.110004
6. Arivazhagan S, Naseer KA, Mahmoud KA et al (2022) Gamma-ray protection capacity evaluation and satellite data based mapping for the limestone, charnockite, and gneiss rocks in the Sirugudi taluk of the Dindigul district, India. Radiat Phys Chem 196:110108. https://doi.org/10.1016/j.radphyschem.2022.110108
7. Kavaz E, Tekin HO, Kilic G, Susoy G (2020) Newly developed Zinc-Tellurite glass system: An experimental investigation on impact of Ta_2O_5 on nuclear radiation shielding ability. J Non Cryst Solids 544:120169. https://doi.org/10.1016/j.jnoncrysol.2020.120169
8. Saritha D, Markandeya Y, Salagram M et al (2008) Effect of Bi_2O_3 on physical, optical and structural studies of ZnO-Bi_2O_3-B_2O_3 glasses. J Non Cryst Solids 354:5573–5579. https://doi.org/10.1016/j.jnoncrysol.2008.09.017
9. Ganguli M, Rao KJ (1999) Structural Role of PbO in Li_2O-PbO-B_2O_3 Glasses. J Solid State Chem 145:65–76. https://doi.org/10.1006/jssc.1999.8221
10. Ichoja A, Hashim S, Ghoshal SK et al (2018) Physical, structural and optical studies on magnesium borate glasses doped with dysprosium ion. J Rare Earths 36:1264–1271. https://doi.org/10.1016/j.jre.2018.05.013
11. Albarzan B, Almuqrin AH, Koubisy MS et al (2021) Effect of Fe_2O_3 doping on structural, FTIR and radiation shielding characteristics of aluminium-lead-borate glasses. Prog Nucl Energy 141:103931. https://doi.org/10.1016/j.pnucene.2021.103931
12. Makarious AS, Bashter II, Abdo AES et al (1996) On the utilization of heavy concrete for radiation shielding. Ann Nucl Energy 23:195–206. https://doi.org/10.1016/0306-4549(95)00021-1
13. Özen S, Şengül C, Erenoğlu T et al (2016) Properties of Heavyweight Concrete for Structural and Radiation Shielding

Purposes. Arab J Sci Eng 41:1573–1584. https://doi.org/10.1007/s13369-015-1868-6
14. Sakr K, El-Hakim E (2005) Effect of high temperature or fire on heavy weight concrete properties. Cem Concr Res 35:590–596. https://doi.org/10.1016/j.cemconres.2004.05.023
15. Singh K, Singh H, Sharma G et al (2005) Gamma-ray shielding properties of CaO-SrO-B_2O_3 glasses. Radiat Phys Chem 72:225–228. https://doi.org/10.1016/j.radphyschem.2003.11.010
16. Libeesh NK, Naseer KA, Arivazhagan S et al (2022) Multispectral remote sensing for determination the Ultra-mafic complexes distribution and their applications in reducing the equivalent dose from the radioactive wastes. Eur Phys J Plus 137:267. https://doi.org/10.1140/epjp/s13360-022-02473-5
17. Lakshminarayana G, Baki SO, Kaky KM et al (2017) Investigation of structural, thermal properties and shielding parameters for multicomponent borate glasses for gamma and neutron radiation shielding applications. J Non Cryst Solids 471:222–237. https://doi.org/10.1016/j.jnoncrysol.2017.06.001
18. Dong MG, Sayyed MI, Lakshminarayana G et al (2017) Investigation of gamma radiation shielding properties of lithium zinc bismuth borate glasses using XCOM program and MCNP5 code. J Non Cryst Solids 468:12–16. https://doi.org/10.1016/j.jnoncrysol.2017.04.018
19. Wagh A, Sayyed MI, Askin A et al (2019) Influence of RE oxides (Eu^{3+}, Sm^{3+}, Nd^{3+}) on gamma radiation shielding properties of lead fluoroborate glasses. Solid State Sci 96:105959. https://doi.org/10.1016/J.SOLIDSTATESCIENCES.2019.105959
20. Naseer KA, Marimuthu K, Al-Buriahi MS et al (2021) Influence of Bi_2O_3 concentration on barium-telluro-borate glasses: Physical, structural and radiation-shielding properties. Ceram Int 47:329–340. https://doi.org/10.1016/j.ceramint.2020.08.138
21. Libeesh NK, Naseer KA, Arivazhagan S et al (2022) Characterization of Ultramafic–Alkaline–Carbonatite complex for radiation shielding competencies: An experimental and Monte Carlo study with lithological mapping. Ore Geol Rev 142:104735. https://doi.org/10.1016/j.oregeorev.2022.104735
22. Sayyed MI, Dwaikat N, Mhareb MHA et al (2022) Effect of TeO_2 addition on the gamma radiation shielding competence and mechanical properties of boro-tellurite glass: an experimental approach. J Mater Res Technol 18:1017–1027. https://doi.org/10.1016/j.jmrt.2022.02.130
23. Arunkumar S, Naseer KA, YoosufAmeen M et al (2023) Physical, structural, optical, and radiation screening studies on Dysprosium ions doped Niobium Bariumtelluroborate glasses. Radiat Phys Chem 204:110669. https://doi.org/10.1016/j.radphyschem.2022.110669
24. Bassam SA, Naseer KA, Keerthana VK et al (2023) Physical, structural, elastic and optical investigations on Dy^{3+} ions doped boro-tellurite glasses for radiation attenuation application. Radiat Phys Chem 110798. https://doi.org/10.1016/j.radphyschem.2023.110798
25. Teresa PE, Naseer KA, Piotrowski T et al (2021) Optical properties and radiation shielding studies of europium doped modifier reliant multi former glasses. Optik (Stuttg) 247:168005. https://doi.org/10.1016/j.ijleo.2021.168005
26. Naseer KA, Marimuthu K (2021) The impact of Er/Yb co-doping on the spectroscopic performance of bismuth borophosphate glasses for photonic applications. Vacuum 183:109788. https://doi.org/10.1016/j.vacuum.2020.109788
27. Naseer KA, Marimuthu K, Mahmoud KA, Sayyed MI (2021) Impact of Bi_2O_3 modifier concentration on barium–zincborate glasses: physical, structural, elastic, and radiation-shielding properties. Eur Phys J Plus 136:116. https://doi.org/10.1140/epjp/s13360-020-01056-6
28. Ibrahim S, El-Agawany FI, Rammah YS et al (2021) ZnO-Bi_2O_3-B_2O_3 glasses doped with rare earth oxides: Synthesis, physical, structural characteristics, neutron and photon attenuation attitude. Optik (Stuttg) 243:167414. https://doi.org/10.1016/j.ijleo.2021.167414
29. Prabhu NS, Hegde V, Sayyed MI et al (2019) Investigations on structural and radiation shielding properties of Er^{3+} doped zinc bismuth borate glasses. Mater Chem Phys 230:267–276. https://doi.org/10.1016/j.matchemphys.2019.03.074
30. Naseer KA, Arunkumar S, Marimuthu K (2019) The impact of Er3+ ions on the spectroscopic scrutiny of Bismuth bariumtelluroborate glasses for display devices and 1.53 µm amplification. J Non Cryst Solids 520:119463. https://doi.org/10.1016/j.jnoncrysol.2019.119463
31. Mhareb MHA (2020) Physical, optical and shielding features of Li_2O–B_2O_3–MgO–Er_2O_3 glasses co-doped of Sm_2O_3. Appl Phys A Mater Sci Process 126. https://doi.org/10.1007/s00339-019-3262-9
32. Chimalawong P, Kirdsiri K, Kaewkhao J, Limsuwan P (2012) Investigation on the Physical and Optical Properties of Dy^{3+} Doped Soda-Lime-Silicate Glasses. Procedia Eng 32:690–698. https://doi.org/10.1016/j.proeng.2012.01.1328
33. Halimah MK, Faznny MF, Azlan MN, Sidek HAA (2017) Optical basicity and electronic polarizability of zinc borotellurite glass doped La^{3+} ions. Results Phys 7:581–589. https://doi.org/10.1016/j.rinp.2017.01.014
34. Dimitrov V, Sakka S (1996) Linear and nonlinear optical properties of simple oxides. II J Appl Phys 79:1741–1745. https://doi.org/10.1063/1.360963
35. Singh DP, Pal Singh G (2013) Conversion of covalent to ionic behavior of Fe_2O_3-CeO_2-PbO-B_2O_3 glasses for ionic and photonic application. J Alloys Compd 546:224–228. https://doi.org/10.1016/j.jallcom.2012.08.105
36. Çelikbilek Ersundu M, Ersundu AE, Sayyed MI et al (2017) Evaluation of physical, structural properties and shielding parameters for K_2O–WO_3–TeO_2 glasses for gamma ray shielding applications. J Alloys Compd 714:278–286. https://doi.org/10.1016/j.jallcom.2017.04.223
37. Kaur S, Arora D, Kumar S et al (2018) Blue-yellow emission adjustability with aluminium incorporation for cool to warm white light generation in dysprosium doped borate glasses. J Lumin 202:168–175. https://doi.org/10.1016/j.jlumin.2018.05.034
38. Agarwal A, Sheoran A, Sanghi S et al (2010) Structural investigation and electron paramagnetic resonance of vanadyl doped alkali niobium borate glasses. Spectrochim Acta Part A Mol Biomol Spectrosc 75:964–969. https://doi.org/10.1016/j.saa.2009.12.003
39. Krishna Mohan N, Sahaya Baskaran G, Veeraiah N (2006) Dielectric and spectroscopic properties of PbO-Nb2O5 -P2O5:V2O5 glass system. Phys Status Solidi 203:2083–2102. https://doi.org/10.1002/pssa.200622093
40. Sathiyapriya G, Divina R, Marimuthu K et al (2021) Exploration on dysprosium ions doped zinc barium boro-tellurite glasses towards radiation screening and photonic applications. Phys B Condens Matter 612:412991. https://doi.org/10.1016/j.physb.2021.412991
41. Reddy R, Nazeer Ahammed Y, Rama Gopal K, Raghuram D (1998) Optical electronegativity and refractive index of materials. Opt Mater (Amst) 10:95–100. https://doi.org/10.1016/S0925-3467(97)00171-7
42. Chen Q, Naseer KA, Marimuthu K et al (2021) Influence of modifier oxide on the structural and radiation shielding features of Sm^{3+}-doped calcium telluro-fluoroborate glass systems. J Aust Ceram Soc 57:275–286. https://doi.org/10.1007/s41779-020-00531-8
43. Bhatia B, Meena SL, Parihar V, Poonia M (2015) Optical Basicity and Polarizability of Nd^{3+}-Doped Bismuth Borate Glasses. New J Glas Ceram 05:44–52. https://doi.org/10.4236/njgc.2015.53006

44. Makishima A, Mackenzie JD (1973) Direct calculation of Young's moidulus of glass. J Non Cryst Solids 12:35–45. https://doi.org/10.1016/0022-3093(73)90053-7
45. Sayyed MI, Issa SAM, Tekin HO, Saddeek YB (2018) Comparative study of gamma-ray shielding and elastic properties of BaO–Bi_2O_3–B_2O_3 and ZnO–Bi_2O_3–B_2O_3 glass systems. Mater Chem Phys 217. https://doi.org/10.1016/j.matchemphys.2018.06.034
46. Sathiyapriya G, Naseer KA, Marimuthu K et al (2021) Structural, optical and nuclear radiation shielding properties of strontium barium borate glasses doped with dysprosium and niobium. J Mater Sci Mater Electron 32:8570–8592. https://doi.org/10.1007/s10854-021-05499-0
47. Kumar M, Rao AS (2020) Concentration-dependent reddish-orange photoluminescence studies of Sm^{3+} ions in borosilicate glasses. Opt Mater (Amst) 109:110356. https://doi.org/10.1016/j.optmat.2020.110356
48. Naseer KA, Sathiyapriya G, Marimuthu K et al (2022) Optical, elastic, and neutron shielding studies of Nb2O5 varied Dy^{3+} doped barium-borate glasses. Optik (Stuttg) 251:168436. https://doi.org/10.1016/j.ijleo.2021.168436
49. Poojha MKK, Naseer KA, Al-Ghamdi H et al (2022) A complete analysis of the structural, optical, and gamma-ray attenuation of Dy^{3+} doped modifiers dependent Lead phosphate boro-tellurite glasses. Optik (Stuttg) 264:169433. https://doi.org/10.1016/j.ijleo.2022.169433
50. Şakar E, Özpolat ÖF, Alım B et al (2020) Phy-X / PSD: Development of a user friendly online software for calculation of parameters relevant to radiation shielding and dosimetry. Radiat Phys Chem 166:108496. https://doi.org/10.1016/j.radphyschem.2019.108496
51. Al-Hadeethi Y, Sayyed MI (2020) BaO–Li_2O–B_2O_3 glass systems: Potential utilization in gamma radiation protection. Prog Nucl Energy 129:103511. https://doi.org/10.1016/j.pnucene.2020.103511
52. Al-Hadeethi Y, Sayyed MI (2020) Evaluation of gamma ray shielding characteristics of CaF_2–BaO –P_2O_5 glass system using Phy-X / PSD computer program. Prog Nucl Energy 126:103397. https://doi.org/10.1016/j.pnucene.2020.103397
53. Abouhaswa AS, El-Agawany FI, Ahmed EM, Rammah YS (2022) Optical, magnetic characteristics, and nuclear radiation shielding capacity of newly synthesized barium boro-vanadate glasses: B2O3–BaF2–Na2O–V2O5. Radiat Phys Chem 192:109922. https://doi.org/10.1016/j.radphyschem.2021.109922